Forensic Science International 245 (2014) 17–23

Contents lists available at ScienceDirect

Forensic Science International

journal homepage: www.elsevier.com/locate/forsciint

Technical Note

Detection of single graves by airborne hyperspectral imaging

G. Leblanc [a,b,*], M. Kalacska [b,1], R. Soffer [a]

[a] National Research Council Canada, Aerospace, Flight Research Laboratory, 1920 Research Road, Building U-61, Ottawa, ON K1A 0R6, Canada
[b] Department of Geography, McGill University, 805 Sherbrooke Street West, Montreal, QC H3A 2K6, Canada

ARTICLE INFO

Article history:
Received 29 July 2013
Received in revised form 17 June 2014
Accepted 19 August 2014
Available online 29 August 2014

Keywords:
Hyperspectral
Grave detection
Single burial
Airborne remote sensing

ABSTRACT

Airborne hyperspectral imaging (HSI) was assessed as a potential tool to locate single grave sites. While airborne HSI has shown to be useful to locate mass graves, it is expected the location of single graves would be an order of magnitude more difficult due to the smaller size and reduced mass of the targets. Two clearings were evaluated (through a blind test) as potential sites for containing at least one set of buried remains. At no time prior to submitting the locations of the potential burial sites from the HSI were the actual locations of the sites released or shared with anyone from the analysis team.

The two HSI sensors onboard the aircraft span the range of 408–2524 nm. A range of indicators that exploit the narrow spectral and spatial resolutions of the two complimentary HSI sensors onboard the aircraft were calculated. Based on the co-occurrence of anomalous pixels within the expected range of the indicators three potential areas conforming to our underlying assumptions of the expected spectral responses (and spatial area) were determined. After submission of the predicted burial locations it was revealed that two of the targets were located within GPS error (10 m) of the true burial locations. Furthermore, due to the history of the TPOF site for burial work, investigation of the third target is being considered in the near future. The results clearly demonstrate promise for hyperspectral imaging to aid in the detection of buried remains, however further work is required before these results can justifiably be used in routine scenarios.

1. Introduction

In studies where airborne detection of clandestine mass graves has shown promise [1,2], the use of hyperspectral imaging (HSI) systems and data analysis has been the key technology. Although sparse in number, these studies illustrate that with sufficient grave material, HSI has the ability to provide a location of potential mass grave sites. However, there has been no work, that the authors are aware of, that uses airborne HSI for detection of single grave sites. A preliminary look at in situ hyperspectral data collected over single graves had shown inconclusive results [1]. Fundamentally, with a single grave there is a much smaller amount of remains when compared to the mass grave studies; thus the probability of detection is lower. As the HSI detection scenario for the mass graves is already challenging, using the same technology for detection of single graves is expected to be an order of magnitude more difficult.

Originally developed for the Earth Sciences [3], HSI has gained popularity within the forensic community for a variety of applications such as trace evidence analysis [4], blood stain ageing [5], chemical identification [6], document analysis [7], and artwork analysis [8], among others. Conceptually, the process of HSI measurement is simple: incoming electromagnetic energy impinges upon a pixel of the detector and generates a voltage which is measured and transformed into a Digital Number (DN). DN's are the basis of the usable HSI data and are converted to Spectral Radiance Units (SRU's) via laboratory-based spectral calibration coefficients determined prior to data collection [9]. Higher order spectral processing is undertaken after the data is converted to SRU units.

For imagery collected from an aircraft or spaceborne platform the spectral HSI results are then georectified to allow for proper mapping of each image onto the surface of the Earth. In the process of georecitfication, the Inertial Navigation System/Global Positioning System (INS/GPS) data collected simultaneously with the imagery allows for distortion corrections due to aircraft motion.

* Corresponding author at: National Research Council Canada, Aerospace, Flight Research Laboratory, 1920 Research Road, Building U-61, Ottawa, ON K1A 0R6, Canada. Tel.: +1 613 998 3525; fax: +1 613 952 1704.
E-mail addresses: George.Leblanc@nrc-cnrc.gc.ca (G. Leblanc), margaret.kalacska@mcgill.ca (M. Kalacska), Ray.Soffer@nrc-cnrc.gc.ca (R. Soffer).
[1] Tel.: +1 514 398 4347; fax: +1 514 398 7437.

http://dx.doi.org/10.1016/j.forsciint.2014.08.020
0379-0738/

However, georectification changes the spectra [10] in each pixel, therefore we have applied the spectral filtering on the un-georectified data, and then applied the spatial filter to the geocorrected data to avoid this problem. The resulting data generally also requires orthorectification; a process often contained within the overall georectification process that takes into account use of a digital elevation model of the topography [11] for proper placement of image pixels.

The purpose of this project was to perform a blind-test of the potential for airborne HSI technology to locate known buried remains of pig carcasses that are used as human analogues. The Royal Canadian Mounted Police (RCMP) supplied two defined areas within the Technical and Protective Operations Facility (TPOF) site in Ottawa, Ontario, Canada, where one area contained no buried remains and the other contained the remains of at least one buried pig. The goal was to collect airborne HSI data and predict the coordinates for the estimated location(s) of the remains and compare those results with the known coordinates. The location(s) of the true remains were only known to the RCMP and at no time during this project were these locations or the age(s) of the burial(s) revealed to the project personnel.

2. Materials and methods

2.1. Site

The TPOF site is located within the semi-urban outskirts of Ottawa, Canada. The site itself consists of mixed-wood forest and clearings. Based on intelligence from the RCMP, the site was reduced from the entire TPOF area to two regions of interest (white boxes in Fig. 1) each of which was nominally 85 m × 35 m and were both within clearings. Arboreal vegetation in the clearings consists predominantly of boreal forest broadleaf and coniferous trees with a mixed herbaceous understory. The soil at the two areas of interest is primarily composed of fine sand with clay horizons expressed at a variety of depths.

2.2. Airborne HSI collection

In areas of basic research where the spectral bands of interest are not well known (as is the case in this work) a hyperspectral imager is far more useful than a multispectral imager due entirely to the fact that a hyperspectral imager gathers much more information with which to evaluate. When the spectral bands of interest are well known, then a multispectral instrument "tuned" to the bands of interest can be used and is a much more efficient method of imaging at that point.

The National Research Council of Canada's Twin Otter was outfitted with two HyperSpectral Imaging (HSI) systems each recording a different but complementary portion of the reflective electromagnetic spectrum from 408 nm to 2524 nm.

The Compact Airborne Spectrographic Imager (CASI) measured the reflective EM spectrum from 408 nm to 905 nm. It is a pushbroom style HSI system with 512 spatial pixels across the flight line covering a Field of View (FOV) of 33.4°. Each spatial pixel has up to 288 spectral channels. However, the full 512 pixels can only be achieved in the 'multispectral mode' resulting in a coarse spectral sampling interval that was considered unacceptable for this project. In 'spectral mode', the full 288 spectral channels can be acquired in only a limited number of spatial pixels. The reduction in spatial information allows more spectral pixels to be acquired. The number of spatial pixels across the flight line determines the minimum sensor integration time (the time allowed for the reflected light to be collected), or the maximum frame rate. The greater the number of spatial pixels the greater will be the time required to read the data out. This leads to larger along-track (i.e. in the direction of flight) pixels because the aircraft is in constant motion as the data is being acquired. As the imaging data requires georectification, the CASI system had its own dedicated GPS/INS system (Novatel) independently collecting the GPS/INS data.

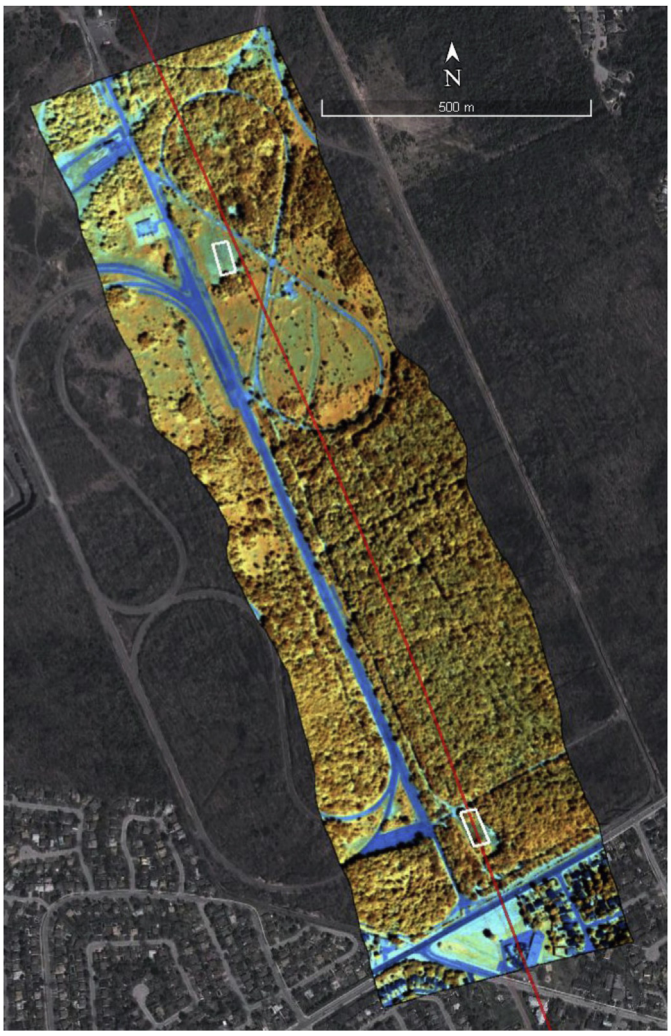

Fig. 1. Three band composite overlay of one of the SASI flight lines in Google Earth. The red line represents the flight path of the aircraft. The white rectangles represent the two areas of interest; the Northern and Southern sites.

The second HSI sensor on board, the Shortwave Airborne Spectrographic Imagery (SASI) is also a push-broom style HSI system that measures the reflective EM spectrum from 883 nm to 2524 nm thus allowing for an overlap region with the CASI data for comparison. The SASI operates in a single configuration acquiring 640 spatial pixels across the flight line covering a FOV of 37.8°. Each spatial pixel has 160 contiguous spectral channels providing a spectral sampling and resolution of approximately 10 nm. Although the SASI integration time is adjustable between 0.5 and 16.7 ms (in order to optimize the measured signal levels) its frame rate is fixed at 60 Hz. Consequently, the along-track spatial resolution is dependent upon the aircraft ground speed and altitude above ground level and only minimally influenced by the applied integration time. The SASI is equipped with its own dedicated GPS/INS system (C-MIGITS III) which collects data used for georectification.

At a flight altitude of 643 m (AGL) the CASI cross track resolution was 0.75 m for each pixel. Given the narrow width of the

study sites (~35 m) 133 CASI spatial pixels were required to ensure coverage when taking into account aircraft positional and attitude errors. For 133 spatial pixels a total of 48 spectral channels were used giving a minimum integration time of 22 ms that resulted in an along-track resolution of 1.28 m.

An aircraft ground speed of 41 m/s was selected providing a SASI cross-track (perpendicular to the flight direction) pixel resolution of 0.69 m. The frame rate for the SASI is set at 60 Hz and at an altitude of 643 m (AGL), results in pixels having an aspect ratio close to one (square pixels) based upon the resulting across-track resolution of the SASI instrument.

The airborne HSI data were collected on July 20th and August 5th, 2011 over the TPOF site (Fig. 1) with concurrent ground HSI data collected the day of the July campaign.

It is clear from the description above that many different aspects of airborne data collection must be considered when planning these missions – aircraft altitude and speed – and in the case of this work, using two different sensors with different parameters (FOV, number of pixels, frame rate, etc.) only compounds the issue. We have attempted to minimize the compromises necessary when engaging in an airborne campaign.

2.3. Ground-based hyperspectral data collection

Spectral data of the asphalt road next to the two fields with the potential grave sites were collected with an ASD Fieldspec3 spectroradiometer concurrent with the July HSI collection. The FieldSpec3™ (Analytical Spectral Devices, Boulder CO.) is a portable high-resolution spectroradiometer that measures reflected electromagnetic radiation within the 350–2500 nm range. The instrument is a single point collection system with three detectors that uses fifty seven fibre optic strands bundled together to collect the reflected electromagnetic energy within the operating range. The input energy undergoes a number of internal corrections (radiometric) and is resampled to output values of approximately 1.0 nm which provides 2150 spectral sample points. The purpose of collecting these ground data was to be able to calibrate and correct for the residual atmospheric effects in the airborne data that standard HSI atmospheric correction (described below) cannot remove.

2.4. HSI preprocessing

One of the greatest challenges with any airborne HSI system is that, due to the high data rate, the instrumentation produces a tremendous amount of data. For example, the SASI alone generates approximately 36GB of data per flight hour. This large volume of data handling requires a significant investment in capital and labour resources. The large data volume is apparent during the preprocessing stage because the entire flight line needs to be corrected before any partitioning into areas of interest can be done.

The first step in the preprocessing consisted of converting the HSI raw digital numbers (DNs) to radiance values (in units of $\mu W\ m^{-2}\ nm^{-1}\ sr^{-1}$) via application of in-lab generated radiometric correction coefficients. These data were converted to reflectance using the FLAASH (Fast Line of Sight Atmospheric Analysis of Spectral Hypercubes) atmospheric correction module resulting in pixel units of ground reflectance in ENVI 4.8 [17,18]. The purpose of the atmospheric correction procedure is to convert the imagery provided as at-sensor-radiance (obtained by the airborne sensors) to surface reflectance thereby removing the majority of the atmospheric effects of absorption and scattering. The module derives surface reflectance by implementing the MODTRAN4 radiative transfer model [19,20]. The model considers the viewing and solar angles and the mean surface elevation. The viewing and solar angles are determined from the date, time and positional information provided. The calculations also require information about the local atmospheric conditions (visibility). The Mid-Latitude Summer (MLS) atmospheric model was chosen as the images were collected in the summer at 45 N latitude which is midway between the MLS (40 N) and Sub-Arctic Summer (50 N) models. The mean surface air temperature for the MLS model is 21 °C as opposed to 14 °C for the SAS. The 5-year mean air temperature for the months of July and August (2007–2011) was 21 °C and 20 °C respectively [12], thus the MLS model was chosen. The rural aerosol model was selected as the study site is a large rural area on the outskirts of Ottawa.

Airborne sensors almost always do not have the same dynamic range and resolution as their ground counterparts. Comparison of ground and airborne data is therefore difficult but necessary. A method to correct for the offset between the airborne and ground spectra is the use of the vicarious calibration method [13–16]. In this method the ground data is taken as "truth" and through a simple ratio correction coefficients are applied to the airborne data. The result is a normalization of the airborne data to the ground data. Geocorrection was not applied until after all the analyses were complete.

2.5. Analysis

The approach taken for this analysis was to exploit the fine spatial and spectral resolutions of the HSI in the calculation of narrow band indices. It is important to note that narrow band indices calculated from imagery with a FWHM of 10 nm or less are not the same as the conventional spectral vegetation indices often calculated from satellite platforms. These extant sensors have coarser spectral resolutions which has been shown to be inappropriate for this application [1].

In order to attempt a logical analysis of the factors possibly indicating grave emplacement, it is important to first consider the actual result of the burial activity. In our case it is disturbance of the soil. Our underlying assumptions were: the soil was disturbed at some point prior to the data collection; biomass remains were emplaced; the disturbed soil area would be a small-scale feature and the intelligence provided reduced the search area to the boundaries of the two regions of interest – the northern and southern sites.

As biomass provides nutrient enrichment to the surrounding vegetation [21] we confined our analysis to indicators exploiting the differences between vegetation with the hypothesis that an anomalous indicator would be seen over the potential grave site(s). The act of digging a grave then replacing the soil to cover the remains is likely to produce a difference in ground mineralogy (specifically in clay content) compared to the surrounding surface. We focused on identifying these variations. As we were looking for small geometrical features (i.e. 2 m × 2 m targets) we further confined our search to small anomalies of disturbed soils.

The first data product evaluated provides an indication of relative distribution of the hydroxyl (OH^-) ion that has a diagnostic absorption in the reflectance data at 2200 nm [22], specifically, the Al–OH bond. The hydroxyl ion is important in this study because it is known to be indicative of the presence of clay. Clay is a general term for a variety of fine-grained minerals (silicates, aluminums, iron oxides, etc.) often the result of weathering processes. It is found in varying amounts in nearly all landform environments. We expected the creation of the grave would leave some clay on the surface. Such a relative enhancement of the 2200 nm reflectance data should be evident over potential gravesites.

The first vegetation index we calculated was the Structure Insensitive Pigment Index (SIPI) given in Eq. (1) where ρ is the

resulting amplitude of reflectance at a specific wavelength. This is an index used to infer the ratio of bulk carotenoids to chlorophyll and is somewhat insensitive to changes in canopy structure [23]. This ratio gives an indication of plant stress and general health. An increase in SIPI is indicative of some increase in stress on the vegetation.

$$\frac{\rho 800 - \rho 445}{\rho 800 - \rho 680} \quad (1)$$

The second vegetation index we calculated was the Sum Green Index (SGI). This represents the integral of the scattered light across the 500–600 nm range where larger values are associated with what human eyesight would associate with "brighter green" vegetation [24]. The final vegetation index we calculated is a variation of the narrowband NDVI and is given in Eq. (2) where ρ is the resulting amplitude of reflectance at a specific wavelength [25]. This index is a calculation that represents the growth of healthy vegetation as well as general plant cover. Over areas where there is greater plant material there will be higher NDVI values. Lower values are associated with outcrop or bare soil. As we were looking for disturbed sites where there is a high probability of exposed soil, a lower value of NDVI was assumed to be an indicator of the target of interest.

$$\frac{\rho 750 - \rho 705}{\rho 750 + \rho 705} \quad (2)$$

Several factors in natural and urban environments can produce index values in the ranges we were hypothesizing for the burials. We needed to consider 'positive locations' or 'anomalies' of interest in the landscape as pixels exhibiting the correct range in all (or most) of the indices calculated as well as adhering to an overall size constraint (spatial area covered by the anomalous pixels). In this case because the targets of interest represented single burials we adhered to a size constraint of a maximum size of 4 m^2.

As a means to restrict the total potential positive 'hits' we used a naïve-Bayes classifier to quantify the probability of a pixel being an 'anomaly' based on our hypotheses of the range the various indices may take in the presence of a grave (i.e. $P(X|Y)$ which is the probability of a grave given the pixel values in all indices combined) [26].

While a substantial amount of data was collected and processed during this work, the speed of processing did not provide a significant barrier to the utility of the method. With the algorithm

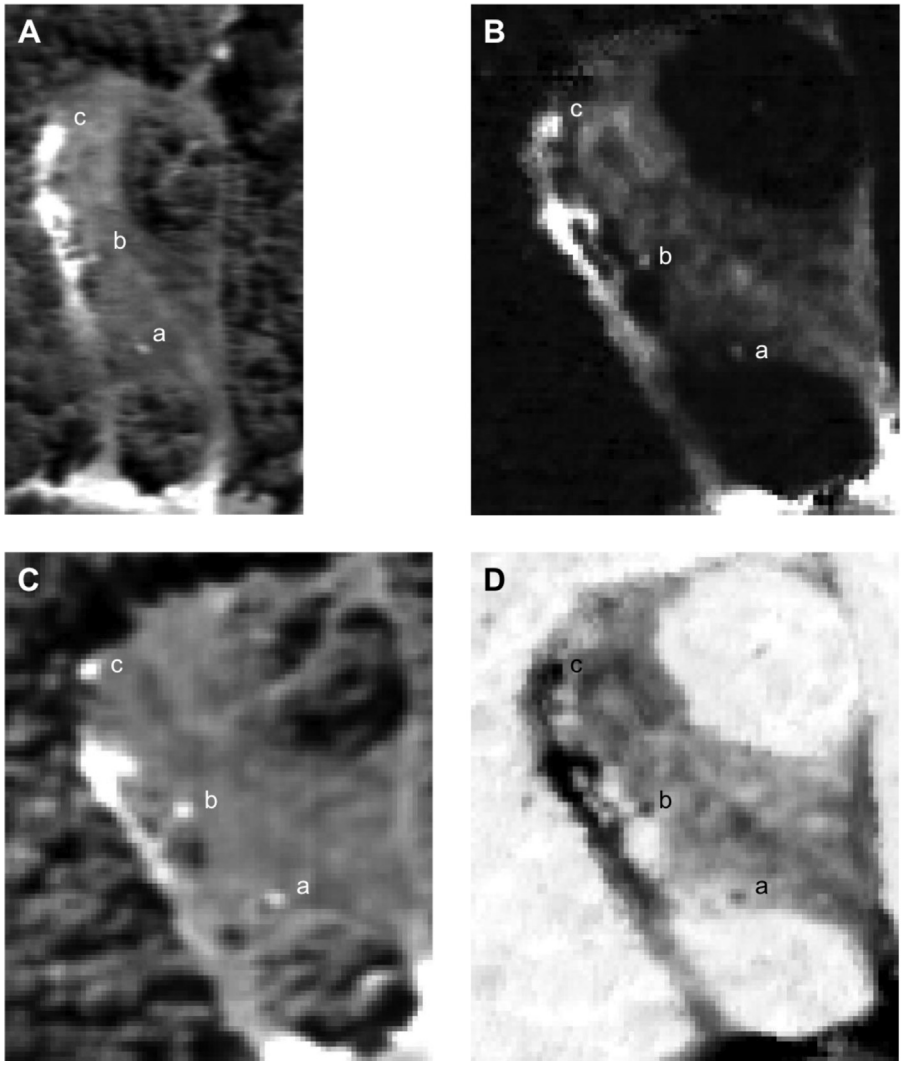

Fig. 2. Results from the various indices visualized independently. (A) Hydroxyl ion (OH^-) from the SASI; (B) SIPI calculated from CASI; (C) SGI calculated from CASI; (D) NDVI calculated from CASI. The three anomalous areas that are present in each index are labelled a, b and c.

in place, the time taken to process the collected information, the intermediary data products and ancillary data (approximately 5GB) for this study was well under 30 min.

3. Results

3.1. Southern site

Our first analysis computed an indication of relative distribution of the hydroxyl (OH^-) ion. The results of the 2203.5 nm data from the SASI system are shown in Fig. 2a. Three potential targets can be seen (labelled a, b and c) conforming to the outlined constraint of overall size of the anomaly. Enhancements can be found around these three targets (24–30%) compared to the background (~19%) (Fig. 2a). The calculation of the SIPI index from the CASI data is shown in Fig. 2b. There are several anomalous values within the site that are both enhanced (light) and reduced (dark). Since we are attempting to identify regions having undergone some amount of disturbance (burial) an increase in SIPI is expected. Anomalous regions of enhanced SIPI values (and within the size constraint) are co-located with the previously identified targets. The results of the SGI calculation are shown in Fig. 2c where three targets can be seen with the above outline in constraints. The targets are higher (0.6–0.8) than the SGI of the background which is 0.03 on average. The results in Fig. 2d show there are a number of reductions in the NDVI values from the average background within the investigation area. Taking into account the considerations of this study (biomass remains and small-scale disturbed soil) we find there are anomalies in NDVI co-located with the other vegetation indices. While there are other anomalies in the NDVI data somewhat similar to the targets a, b and c; there are no significant associated enhancements in the other indices within the search area.

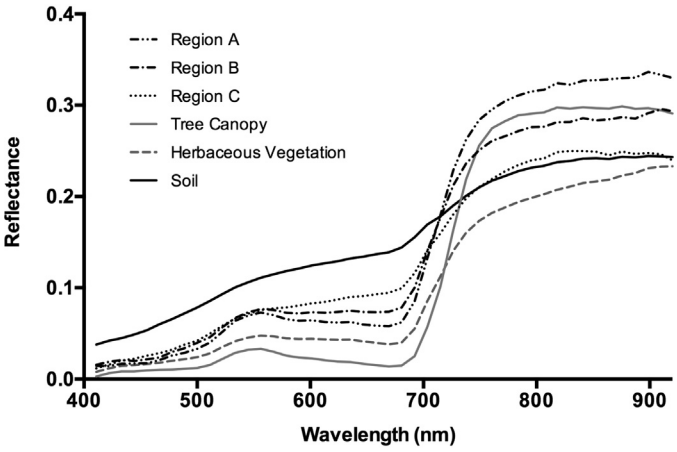

Fig. 3. Spectral signatures from CASI of the three anomalous regions, vegetation classes and soil.

The average spectral signatures of the three anomalous areas (Fig. 3) illustrate a mix between the vegetation classes and the soil in the scene. A three-dimensional scatter plot (Fig. 4) illustrates the distribution of the pixels representing the three targets of interest in comparison to other cover types in the scene; exposed soil, broadleaf tree canopy; and mixed herbaceous vegetation. There is strong separability between this anomalous class of pixels and the three other cover types in the scene based on the values of the three vegetation indices combined. A calculation of the Jeffries–Matusita distance [27] indicates a value of 2.0 between the anomalies and the tree canopy class; 1.97 between the anomaly and the mixed herbaceous class; and 1.88 between the anomaly and exposed soil. The Jeffries–Matusita distance quantifies the

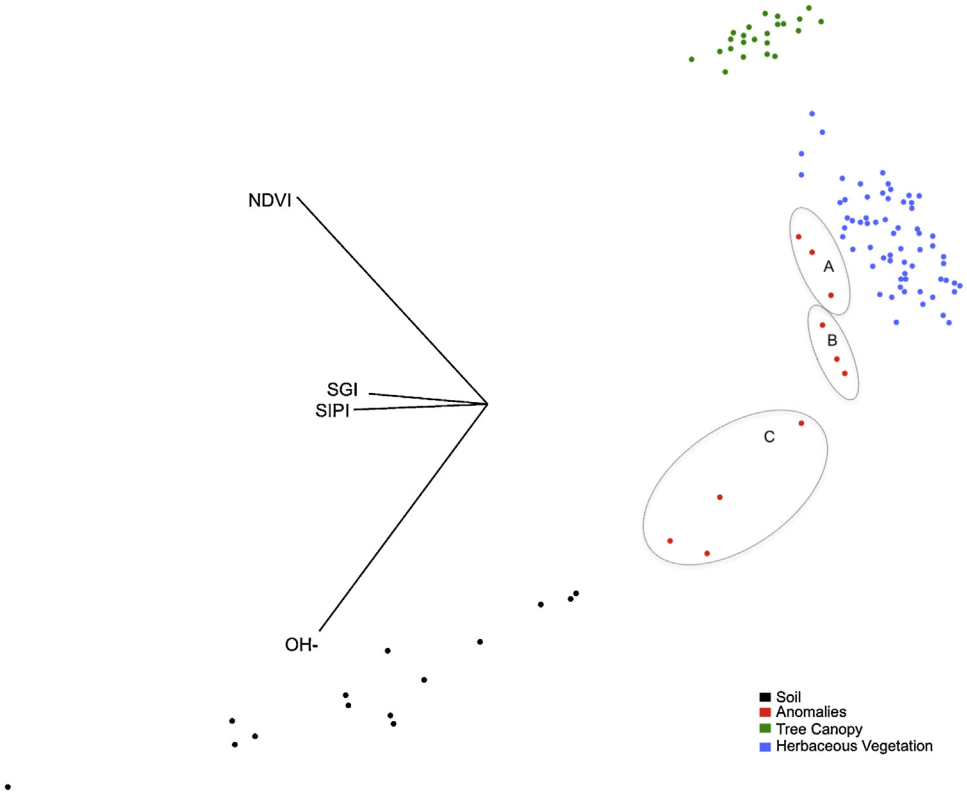

Fig. 4. Four-dimensional scatter plot of the pixels representing soil, tree canopy, herbaceous vegetation and the anomalies (A,–C). The axes represent the four indices calculated from the CASI and SASI sensors. Each point is a pixel.

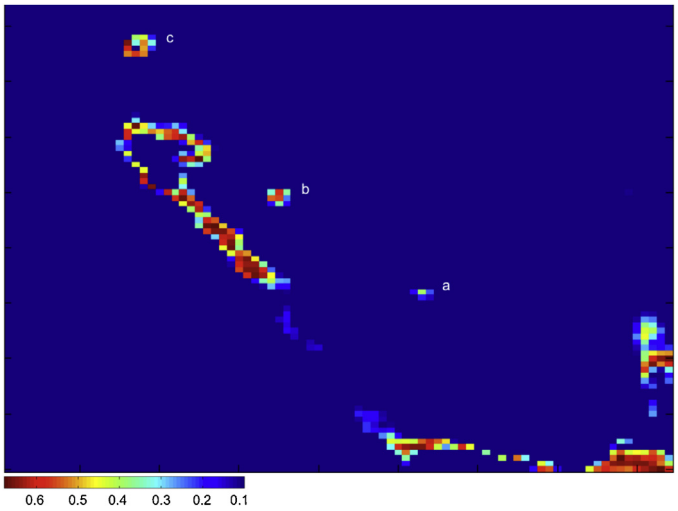

Fig. 5. Bayesian probability map of the Southern site. The scale indicates the probability of a pixel meeting the spectral criteria of an anomaly.

separability (i.e. difference) between various classes. It ranges from 0 to 2 with higher values indicating greater separability. Calculation of the Bayesian probability map (Fig. 5) reveals several pixels within and around the study area having the highest likelihood of pertaining to our anomalous class of interest, however only three (targets a, b, c) adhere to the spatial constraint outlined in our method.

3.2. Northern site

From the data products generated for the northern site of greatest interest is the presence of hydroxyl ion as it is the only one of the four indicators illustrating potential anomalous regions in this area. We were unable to show any uniquely identifiable potential grave locations in this site due to a lack of co-occurrence of anomalous sites in the various indicators (OH^-, SIPI, CGI and NDVI). The Bayesian probability map did not reveal any potential sites that matched the spatial constraint. At this point we suggest the northern site does not contain any burials as we were unable to show any uniquely identifiable potential grave location.

3.3. Validation

After analysis of the data was performed and submitted to the RCMP, the RCMP then confirmed that the northern site did not contain any burials.

From the targets defined in the southern site (targets a, b and c) we noted the location within the geocorrected imagery. The on-board airborne GPS/INS system was not using differential GPS and therefore, position values derived were prone to errors from the atmosphere and measurement of the L2 GPS signal that is typically within the range of 5–10 m. Similar valued errors were also verified for the RCMP hand-held GPS used as the "truth" for the burial locations. The error in the airborne data must be considered when compared to the ground data; as well as the additive errors associated with the ground data. We suggest a very successful trial has been had if the "true" locations are within 10 m of the predicted locations.

The RCMP confirmed the burial locations for targets a and b are within the GPS error of the system, corresponding to known graves 4 years old, and 1 month old, respectively. Target c is located outside of the region of interest of the general study area. Due to the persistent signature of target c and the fact that the TPOF site has been used for several years for forensic experiments and has experienced several burial events which have not been geolocated, it is our intention to investigate target c in the near future to confirm whether actual remains are buried there.

4. Conclusion

This project was a co-operative blind-test of the potential for airborne hyperspectral imaging to detect single graves. It is based upon previous work used for the detection of mass graves [1,2,21]. The test consisted of two sites, one with buried pig carcasses and the other without any burials. During the entire project timeline the locations of the true burial sites were only known to the RCMP. At no time prior to submitting the locations of potential burial sites from the hyperspectral image analysis were the actual locations of the sites released or shared with anyone from the analysis team. Based on the data generated and the interpretations made we suggested the southern site is the one containing the burial of the pig carcasses. Within this site we identified three potential areas conforming to our underlying assumptions of the expected spectral responses; although one of the targets technically lies outside of the given bounds of the area under investigation. We included target c because it is spatially close to the site boundary and continually displayed the same associations between data sets that the other two sites (targets a and b) displayed.

After submission of the predicted burial locations the RCMP released the locations of the actual known burials. It was then revealed the predicted targets a and b were located within GPS positional error to the true burial locations. Due to the history of the TPOF site for burial work and since target c is located outside the general study area, yet retains the same classification as targets a and b, investigation of target c is being considered in the near future.

The results of this work show promise for hyperspectral imaging to aid in the detection of buried remains. Further work is required before these results can justifiably be used in routine scenarios. We suggest follow-on work include:

1) Use of differential GPS for geolocation to much better than the 10 m accuracy;
2) Development and implementation of measurements in various environments – grasslands, cultivated fields, marshes, woods and along roadsides, etc. as different indicators are likely under different environments.

Acknowledgements

The authors would like to thank Dr. Brian Yamashita and Dr. Della Wilkinson from the RCMP for their participation and Dr. Pablo Arroyo for his help in the collection of the field spectra. This project was supported by the Canadian Police Research Centre.

References

[1] M. Kalacska, L.S. Bell, Remote sensing as a tool for the detection of clandestine mass graves, Can. Soc. Forensic Sci. J. 39 (2006) 1–13.
[2] M.E. Kalacska, L.S. Bell, G. Sanchez-Azofeifa, T. Caelli, The application of remote sensing for detecting mass graves: an experimental animal case study from Costa Rica, J. Forensic Sci. 54 (2009) 159–166.
[3] G.B. Bailey, J.L. Dwyer, D.J. Meyer, AVIRIS data characteristics and their effects on spectral discrimination of rocks exposed in the Drum Mountains, Utah: results of a preliminary study, in: Proceedings of the Airborne Visible/Infrared Imaging Spectrometer (AVIRIS) Performance Evaluation Workshop: NASA Jet Propulsion Laboratory, 1988, p. 13.
[4] G.J. Edelman, E. Gaston, T.G. van Leeuwen, P.J. Cullen, M.C.G. Aalders, Hyperspectral imaging for non-contact analysis of forensic traces, Forensic Sci. Int. 223 (2012) 28–39.

[5] G. Edelman, T.G. van Leeuwen, M.C.G. Aalders, Hyperspectral imaging for the age estimation of blood stains at the crime scene, Forensic Sci. Int. 223 (2012) 72–77.
[6] B.K. Alsberg, Is sensing spatially distributed chemical information using sensory substitution with hyperspectral imaging possible, Chemom. Intell. Lab. Syst. 114 (2012) 24–29.
[7] D. Goltz, M. Attas, G. Young, E. Cloutis, M. Bedynski, Assessing stains on historical documents using hyperspectral imaging, J. Cult. Herit. 11 (2010) 19–26.
[8] M. Kubik, Hyperspectral imaging: a new technique for the non-invasive study of artworks, in: C. Dudley, B. David (Eds.), Physical Techniques in the Study of Art, Archaeology and Cultural Heritage, Elsevier, 2007, pp. 199–259 (Chapter 5).
[9] ITRES Research Ltd., SASI Data Standard Processing. Calgary, AB. p. 16.
[10] R. Richter, D. Schläpfer, Geo-atmospheric processing of airborne imaging spectrometry data. Part 2: Atmospheric/topographic correction, Int. J. Remote Sens. 23 (2002) 2631–2649.
[11] J.W. Boardman, Precision geocoding of low-altitude AVIRIS data: lessons learned in 1998, in: Summaries of the Eighth Annual JPL Airborne Geoscience Workshop, JPL Publication, 1999, pp. 63–68.
[12] Canada E., National Climate Data and Information Archive, 2013.
[13] J. Secker, K. Staenz, R.P. Gauthier, P. Budkewitsch, Vicarious calibration of airborne hyperspectral sensors in operational environments, Remote Sens. Environ. 76 (2001) 81–92.
[14] P.M. Teillet, G. Fedosejevs, R.P. Gauthier, N.T. O'Neill, K.J. Thome, S.F. Biggar, et al., A generalized approach to the vicarious calibration of multiple Earth observation sensors using hyperspectral data, Remote Sens. Environ. 77 (2001) 304–327.
[15] H.P. White, K.S. Khurshidt, R. Hitchcock, R. Neville, S. Lixin, C.M. Champagne, et al., From at-sensor observation to at-surface reflectance – calibration steps for Earth observation hyperspectral sensors, in: Geoscience and Remote Sensing Symposium 2004. IGARSS '04. Proceedings 2004 IEEE International, vol. 5, 2004, pp. 3241–3244.
[16] L. Cheng-Chien, A. Kamei, H. Kuo-Hsien, S. Tsuchida, H.M. Huang, S. Kato, et al., Vicarious calibration of the formosat-2 remote sensing instrument, IEEE Trans. Geosci. Remote Sens. 48 (2010) 2162–2169.
[17] G.P. Anderson, B. Pukall, C.L. Allred, L.S. Jeong, M. Hoke, J.H. Chetwynd, et al., FLAASH and MODTRAN4: state-of-the-art atmospheric correction for hyperspectral data, in: Aerospace Conference, 1999 Proceedings 1999 IEEE, vol. 4, 1999, pp. 177–181.
[18] T. Cooley, G.P. Anderson, G.W. Felde, M.L. Hoke, A.J. Ratkowski, J.H. Chetwynd, et al., FLAASH, a MODTRAN4-based atmospheric correction algorithm, its application and validation, in: Geoscience and Remote Sensing Symposium 2002. IGARSS '02. 2002 IEEE International, vol. 3, 2002, 1414–1418.
[19] A. Berk, L.S. Bernstein, G.P. Anderson, P.K. Acharya, D.C. Robertson, J.H. Chetwynd, et al., MODTRAN cloud and multiple scattering upgrades with applications to AVIRIS, Remote Sens. Environ. 65 (1998) 367–3754.
[20] M.W. Matthew, S.M. Adler-Golden, A. Berk, S.C. Richtsmeier, R.Y. Levine, L.S. Bernstein, et al., Status of atmospheric correction using a MODTRAN4-based algorithm, in: SPIE Proceedings, Algorithms for Multispectral, Hyperspectral, and Ultraspectral Imagery VI, 2000, pp. 199–207.
[21] J.C. Calvo-Alvarado, M. Kalacska, G.A. Sanchez-Azofeifa, L.S. Bell, Effect of soil type on plant growth, leaf nutrient/chlorophyll concentration and leaf reflectance of tropical tree and grass species, in: M. Kalacska, G.A. Sanchez-Azofeifa (Eds.), Hyperspectral Remote Sensing of Tropical and Sub-Tropical Forests, Taylor and Francis Group, Boca Raton, FL, 2008, pp. 87–123.
[22] R.N. Clark, T.V.V. King, M. Klejwa, G.A. Swayze, High spectral resolution reflectance spectroscopy of minerals, J. Geophys. Res. 95 (1990) 12653–12680.
[23] J. Penuelas, F. Baret, I. Filella, Semi-empirical indices to assess carotenoids/chlorophyll-a ratio from leaf spectral reflectance, Photosynthetica 31 (1995) 221–230.
[24] D.B. Lobell, G.P. Asner, Hyperion studies of crop stress in Mexico, in: Proceedings of the 12th Annual JPL Airborne Earth Science Workshop, Pasadena, CA, 2003.
[25] D.A. Sims, J. Gamon, Relationships between leaf pigment content and spectral reflectance across a wide range of species, leaf structures and developmental stages, Remote Sens. Environ. 81 (2002) 337–354.
[26] G. John, P. Langley, Estimating continuous distributions in Bayesian classifiers, in: Proceedings of the Eleventh Conference on Uncertainty in Artificial Intelligence, Morgan Kaufmann Publishers, San Mateo, 1995, pp. 338–345.
[27] J.A. Richards, Remote Sensing Digital Image Analysis, Springer-Verlag, Berlin, 1999.